Polymer-Plastics Technology and Engineering, 45: 9–21, 2006

ISSN: 0360-2559 print/1525-6111 online
DOI: 10.1080/03602550500371471

Taylor & Francis
Taylor & Francis Group

Simulation of Nonlinear Polyurethane Production in a Twin-Screw Extruder

René O. Vargas and Eduardo Vivaldo-Lima
Departamento de Ingeniería Química, Facultad de Química, Universidad Nacional Autónoma de México (UNAM), México D.F., México

Octavio Manero
Instituto de Investigaciones en Materiales (IIM), UNAM, México D.F., México

The production of nonlinear polyurethane from the reaction of methyl diisocyanate (MDI) with a mixture of a polyester and 1,4-butanediol was studied in a closely intermeshing, counter-rotating twin-screw extruder, using an ideal reactor model consisting of a series of continuous stirred tank reactors (CSTR) coupled to a previously developed kinetic-probabilistic model. The kinetic part of the model allows for the calculation of concentrations of all species. A recursive probabilistic model is used to calculate the number and weight average molecular weights. Allophanate reactions, as well as gel formation due to crosslinking, are considered in the model. Pressure, flow rate, and polymer properties along the extruder can be calculated with the model.

Keywords Reactive extrusion; Polyurethane; Crosslinking; Twin-screw extruder; Modeling

INTRODUCTION

Reactive extrusion (REX) links two common processes: chemical reaction engineering, represented by polymer synthesis or compounding, and polymer processing. Recently, the industrial use of extruders as polymerization reactors has increased considerably. Technological development advances for single and twin-screw extruders have been reviewed by Rauwendal[1] and White[2]. Extruders have gradually increased their importance in the plastic compounding industry because of their superior mixing capabilities and better control of the residence time distribution. These same attributes are even more valuable in reactive extrusion. Advantages of using extruders as chemical reactors include avoiding using solvents, and the good mixing and heat transfer provided by the mechanical action of the screws, even at high viscosities.

The use of extruders in industry has prompted the development or growth of several research areas, such as mechanisms of polymer melting, compounding, flow behavior, measuring and modeling of residence time distributions, etc.[3–10] The different phenomena that determine the performance and operation of an extruder can be analyzed and better understood by using mathematical models. Potente et al.[5,6,11–13] and Flecke et al.[14] have developed mathematical models for single and co-rotating extruders, which have been used to simulate several processes. Vergnes, Della Valle, and Delamare[15] proposed a global computational model for self-wiping co-rotating twin extruders, which have also been studied by several other research groups[16–18]. Janssen[19,21] and Van der Goot et al.[21,22] have worked extensively with counter-rotating twin extruders.

The production of polyurethane in extruder reactors has been reported by a number of researchers[23–25]. An engineering analysis of the reactive extrusion process of thermoplastic polyurethane, through numerical simulation and experiments, was carried out by Hyun and Kim[26]. The ideal reactor model developed by Janssen[19] for a counter-rotating twin-screw extruder has been well accepted and used in many research studies. Stuber[27] modeled the polymerization of methyl methacrylate, and Jongbloed, Mulder, and Janssen[28] studied the copolymerization of n-butyl methacrylate with 2-hydroxypropyl-methacrylate. Bouilloux and Macosko[23] modeled the production of a linear polyurethane, using the ideal reactor approximation of Janssen[19]. Ganzeveld and Janssen[24] studied the mixing mechanism in the twin extruder. The use of the counter-rotating twin-screw extruder has increased and gained importance. Ganzeveld and Janssen[29] proposed scale-up rules for this kind of machine. Bulk, dispersed phase, and reactive blending

Address correspondence to Eduardo Vivaldo-Lima, Departamento de Ingeniería Química, Facultad de Química, Universidad Nacional Autónoma de México (UNAM), Conjunto E, Ciudad Universitaria, México D.F., CP 04510, México. E-mail: vivaldo@servidor.unam.mx

polymerization of urethane in twin extruders were studied by Cassagnau et al.[30,31] and Deloor et al.[32,33].

Although complex polymer processing units, such as extruders, can in principle be modeled using rigorous models based on the detailed equations of motion and computational fluid dynamics (CFD) techniques, with the aid of commercial software packages such as Fluent or Femlab, the fact is that when complex polymerization schemes are considered and, moreover, if the polymerization kinetics controls the performance of the processing unit, it is still useful to use simplified models for flow along the extruder length to describe the key aspects of the process. This approach makes possible to easily evaluate more rigorous polymerization kinetic models, based on more realistic reaction mechanisms, using fairly simple overall mathematical models and standard computational tools.

In this contribution, nonlinear polyurethane formation in a closely intermeshing, counter-rotating twin-screw extruder is examined, using the ideal reactor approximation model[19,23], coupled to the Macosko-Miller recursive method for calculation on number and weight average molecular weights[34,35] in nonlinear polyurethane production. Conversions of all species, extruder pressure generation, the effect of the stoichiometric ratio, and the gelation point can be calculated with the present model.

DESCRIPTION OF THE MODEL

Flow and Geometric Characteristics of the Extruder

The counter-rotating twin-screw extruder used in this work is of the closely intermeshing type, and consists of a series of C-shaped chambers in which material moves along the extruder length towards the die. Interactions among the chambers occur through leakage gaps. A graphical representation of the flows present in this type of extruder is presented in Fig. 2 of Ganzeveld and Janssen[29]. The leakage gaps are classified in four groups[19], namely: a) flight gap, $\boldsymbol{Q_f}$, which is the clearance between the barrel and the flight of the screws; b) tetrahedron gap, $\boldsymbol{Q_t}$, which is a gap with the shape of a tetrahedron, between the flight walls, and it connects the consecutive chambers on the opposite screws; c) calender gap, $\boldsymbol{Q_c}$, formed by the clearance between the flight of one screw and the bottom of the channel of the other screw, and resembles a calender; and d) side gap, $\mathbf{Q_s}$, which forms between the flanks of the flights of the two screws.

According to Stuber[27] and Bouilloux and Macosko[23], the leakage gap equations can be summarized as follows.

Flow through the flight gap

$$Q_f^i = (2\pi - \alpha)R_e\left\{\frac{NB\delta}{2} + \frac{\delta^3(p^i - p^{i-2})}{12B\eta^i}\right\} \tag{1}$$

Flow through the tetrahedron gap

$$Q_t^i = 0.0054\frac{(p^i - p^{i-1})}{\eta^i}\left(\frac{H}{R_e}\right)\left\{\psi + 2\left(\frac{\varepsilon + \sigma\tan\psi}{H}\right)^2\right\} \times R_e^3(p^i - p^{i-1}) \tag{2}$$

Flow through the calender gap

$$Q_c^i = \frac{4}{3}(B - B_e)\left\{N\pi(2R_e - H)\sigma + \frac{\sigma^3(p^i - p^{i-2})}{6\pi\eta^i[(2R - H)\sigma/2]^{0.5}}\right\} \tag{3}$$

Flow across the side gap

$$Q_s^i = \pi N(2R_e - H)(H - \sigma)(\varepsilon + \sigma\tan\psi) + (p^i - p^{i-2}) \times \frac{(H - \sigma)(\varepsilon + \sigma\tan\psi)^3\cos^2\psi}{12\eta^i} \times \left\{1 - 0.63\frac{(\varepsilon + \sigma\tan\psi)\cos^2\psi}{H - \sigma} + 0.052\left(\frac{(\varepsilon + \sigma\tan\psi)\cos^2\psi}{H - \sigma}\right)^5\right\} \tag{4}$$

The flow interactions among the C-shaped chambers of the counter-rotating twin extruder are shown in Fig. 1. The geometrical constants are shown in Fig. 4 of Ganzeveld and Janssen[29]. The volumetric displacement rate or theoretical throughput, Q_{th}, equals the number of C-shaped chambers transported per unit time, times the chamber volume, as indicated in Eq. (5),

$$Q_{th} = 2\,mN\,V_c \tag{5}$$

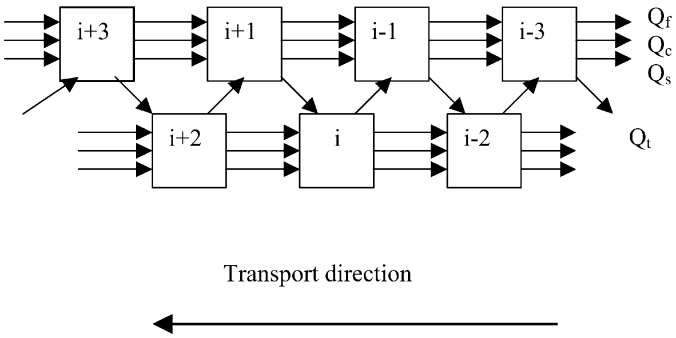

FIG. 1. Flow interactions between C-shaped chambers in a closely intermeshing counter-rotating twin-screw extruder.

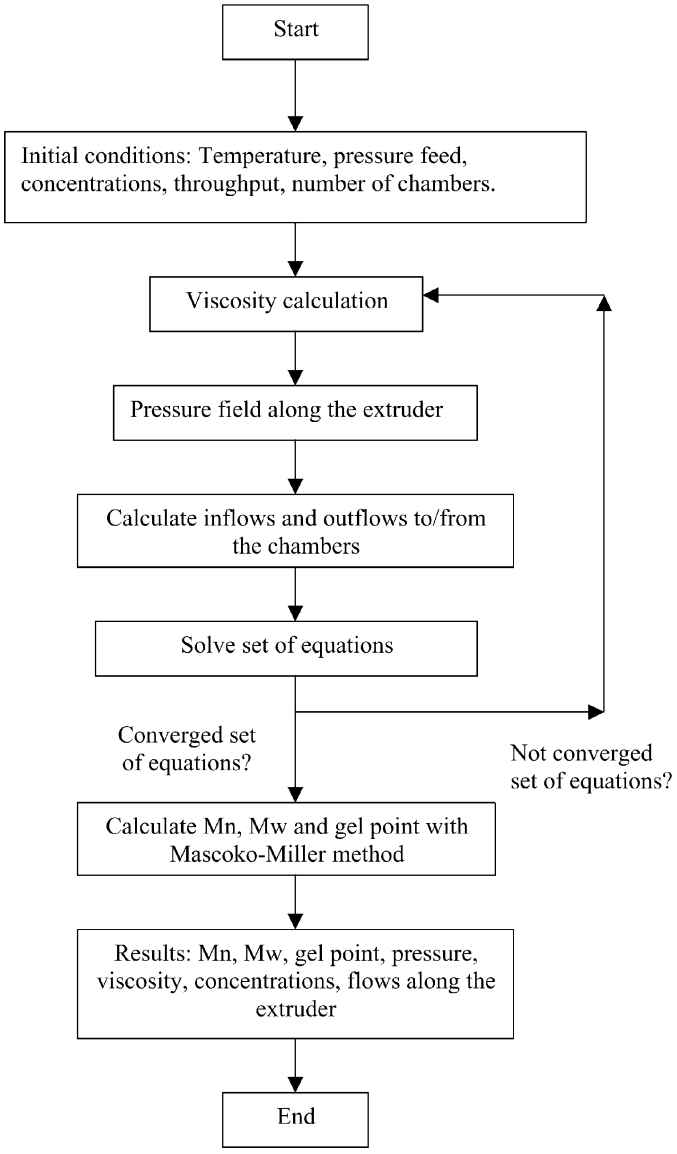

FIG. 2. Flow chart of the numerical simulation.

where m is the number of thread starts, N is the screw rotation rate, and V_c is the volume of a chamber. The actual volumetric throughput is given by Eq. (6).

$$Q = Q_{th} - Q_l \tag{6}$$

Q_t in Eq. (6) is the sum of all leakage flows over a cross section of the extruder, as indicated in Eq. (7).

$$Q_{tot} = Q_t^i + Q_f^i + Q_c^i + Q_s^i \tag{7}$$

The system can be simplified into a set of equations in terms of geometrical constants, pressure, screw speed, and viscosity[23,27]. The three leakage terms, Q_f, Q_c, and Q_s, depend on viscosity, pressure, and screw speed, so that they can be lumped into a single parameter, Q_3, as indicated in Eqs. (8) and (9).

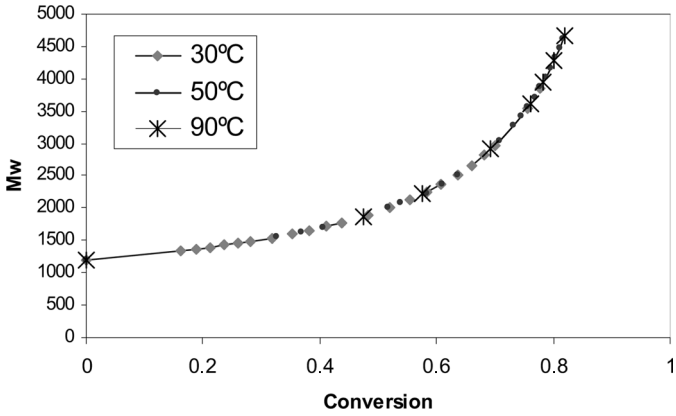

FIG. 3. Copolymerization of MDI/polyol/1,4-Butanediol. Calculated data by Castro[14] for weight average molecular weight. Initial conditions are disclosed in Table 1.

$$Q_3^i = Q_f^i + Q_c^i + Q_s^i \tag{8}$$

$$Q_3^i = (Q3A)N + \frac{(Q3B)(P^i - P^{i-2})}{\eta^i} \tag{9}$$

The tetrahedral gap does not depend on N, so that Eq. (10) is more adequate in this case.

$$Q_t^i = \frac{(QTB)(P^i - P^{i-1})}{\eta^i} \tag{10}$$

Subscripts i, i − 1, and i − 2 in Eqs. (8) to (10) denote chambers or CSTRs number i, i − 1, and i − 2, respectively. $Q3A$ is a constant that combines all the drag flow terms of the flight, calender, and side gap leakages. $Q3B$ is a constant

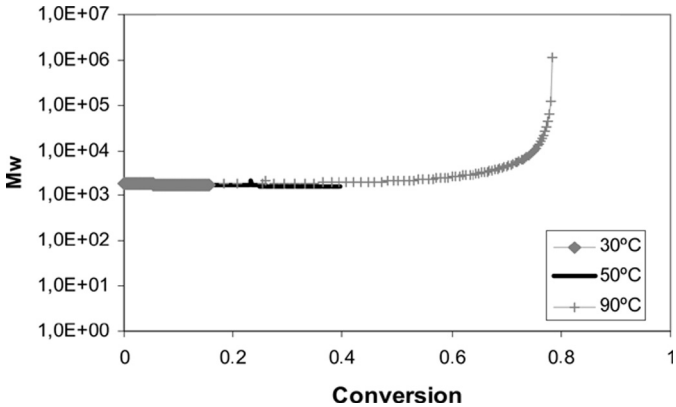

FIG. 4. Copolymerization of MDI/polyol/1,4-Butanediol. Model predictions using the model by Vivaldo-Lima et al.[36] for weight-average molecular weight. Initial conditions as per Table 1.

that combines all the pressure-driven flow terms of the flight, calender, and side gap leakages. QTB is a constant that combines all the pressure-driven flow terms of the tetrahedron gap leakages.

The previous flow equations connecting the chambers were derived considering the following assumptions: a) homogeneous C-shaped chambers, b) all chambers are fully filled, c) uniform extruder configuration, and d) uniform wall temperature.

Using the leakage flow equations, represented by Eqs. (13) to (15), the mass, component, and heat balance equations can be written as indicated in Eqs. (11) to (16), where x in Eq. (14) denotes any component in the system.

$$Q^i_{in} = Q^{i-1}_{forward} = Q^{i-1}_{mechanical} - Q^{i-1}_{leakage} = 2\,NV^{i-1} - Q^{i-1}_t - Q^{i-1}_3 \tag{11}$$

$$Q^i_{out} = Q^i_{forward} + Q^i_3 = 2\,NV^i - Q^i_t \tag{12}$$

Mass balance

$$\frac{d(V^i\rho^i)}{dt} = Q^i_{in}\rho^{i+1} + Q^{i+1}_3\rho^{i+1} - Q^i_{out} \tag{13}$$

Component balance

$$\frac{d(V^i x^i)}{dt} = Q^i_{in}x^{i-1} + Q^{i+1}_3 x^{i+1} - Q^i_{out}x^i + V^i(rate)^i \tag{14}$$

Heat balance

$$\frac{d(V^i\rho CpT^i)}{dt} = Q^i_{in}\rho^{i-1}CpT^{i-1} + Q^{i+1}_3\rho^{i+1}CpT^{i+1} - Q^i_{out}\rho^i CpT^i + V^i\Delta HpKp[NCO]_0 + UR(S-B)(2\pi-\alpha)(Twall - T^i) \tag{15}$$

Net forward mass flow balance across any cross-section

$$\text{Forward mass flow rate} = (2\,NV^i - Q^i_t - Q^i_3)\rho^i - Q^{i+1}_3\rho^{i+1} \tag{16}$$

Using a kinetic-probabilistic approach for nonlinear polyurethane production kinetics and molecular weight development[36], coupled to the extruder equations, the polymerization properties along the extruder barrel can be calculated.

Kinetic-Probabilistic Description of Polymerization

The polymerization model used in this paper[36] consists of a set of kinetic equations that describe the rates of consumption or formation of all the species present in the system, and a set of algebraic equations, an application of the recursive probabilistic model of Macosko-Miller[34,35] to this reacting system, which allows for calculation of the molecular weight averages and the gelation point. Although the extruder chambers are modeled as CSTRs, and a model based on probabilistic arguments for a batch reactor may not be applicable to a CSTR, a series of CSTRs approximate the behavior of a plug flow reactor (PFR), which can be approximated with the same probabilistic arguments as a batch reactor, for molecular weight distribution (MWD) calculation purposes. Therefore, usage of the Macosko-Miller recursive probabilistic approach for calculation of M_w and the gelation point seems adequate.

The reaction scheme used here is similar to that used by Gupta and Kumar[37], except for the reactions with a low-molecular-weight diol (B'—B'), which were included in the model by Vivaldo-Lima et al.[36]. Another difference is that, in this reaction scheme, hydroxyl groups from different reagents are allowed to have different reactivities. However, all hydroxyl groups of a single molecule have the same reactivity. The reaction scheme, Eqs. (17) to (28), is shown below. Note that, in these equations, a horizontal line represents a polymer chain, and a superscript * on a functional group indicates that the functional group is bound to a polymer chain. Thus, —A^* represents a polymer chain with an A end group, and —AB— represents the linkage of an A functional group with a B functional group located at an intermediate position within a polymer chain.

The reaction scheme used by Vivaldo-Lima et al.[36] was simplified, considering only the reactions described in Eqs. (17) to (28).

$$A_2A_1 + B- \xrightarrow{k_1} {}^*A_2A_1B - (E) \tag{17}$$

$$A_1A_2 + B- \xrightarrow{k_2} {}^*A_1A_2B - (E) \tag{18}$$

$$-A^*_1 + B- \xrightarrow{k^*_1} -A_1B - (E) \tag{19}$$

$$A^*_2 + B- \xrightarrow{k^*_2} -A_2B - (E) \tag{20}$$

Equations (17) to (20) show the four different reactions between isocyanate (A) and hydroxyl (B) functional groups from a diol of high molecular weight to produce a urethane functional group (E). Depending on the values of the kinetic rate constants k_1, k_2, k^*_1, and k^*_2, the cases of equal or unequal reactivities of the isocyanate functional group can be modeled. It is assumed that functional groups bound to a polymer molecule (as indicated by a superscript *) are less reactive than those from a monomer molecule. In the

reaction scheme above, A_1A_2 represents a diisocyanate monomer molecule. Subscripts 1 and 2 identify the individual isocyanate groups belonging to the diisocyanate molecule. As stated before, a superscript * on a functional group indicates that the functional group is bound to a polymer chain. When attached to a kinetic constant, the superscript indicates the reactivity of the functional group attached to a polymer chain, as opposed to that of a functional group belonging to a monomer molecule.

Equations (21) to (24) show the equivalent reactions, but in this case the diol is a low molecular weight molecule (B').

$$A_1A_2 + B' - \xrightarrow{k_3} {}^*A_2A_1B' - (E) \tag{21}$$

$$A_1A_2 + B' - \xrightarrow{k_4} {}^*A_1A_2B' - (E) \tag{22}$$

$$-A_1^* + B' - \xrightarrow{k_3^*} -A_1B' - (E) \tag{23}$$

$$A_2^* + B' - \xrightarrow{k_4^*} -A_2B' - (E) \tag{24}$$

The formation of allophanate functional groups (M) is represented by Eqs. (25) to (28).

$$A_2A_1 + E \xrightarrow{R_3K_1} M(+{}^*A_2-) \tag{25}$$

$$-A_1^* + E \xrightarrow{R_3K_1} M \tag{26}$$

$$-A_1^* + E \xrightarrow{R_3K_1} M \tag{27}$$

$$-A_2^* + E \xrightarrow{R_3K_2} M \tag{28}$$

B represents a hydroxyl functional group from the polyester. B' is a hydroxyl functional group from 1,4-butanediol (low-molecular-weight extender). A diol molecule is made of two hydroxyl functional groups (B—B), and a diisocyanate molecule consists of two isocyanate functional groups. E and M represent the urethane and allophanate functional groups, respectively.

R_3 is a constant that indicates that the rate of allophanate formation is proportional to the rate of urethane production. In other words, the reactivity of an isocyanate functional group with a proton from the urethane group is proportional to the reactivity of an isocyanate group with a hydroxyl functional group. From the reaction scheme represented by Eqs. (17) to (28), the following kinetic equations can be derived in the same way that Vivaldo-Lima et al.[36] did.

$$\frac{d[A_1]}{dt} = -k_1[A_1]([B] + R_3[E]) - k_3[A_1][B'] \tag{29}$$

$$\frac{d[A_2]}{dt} = -k_2[A_2]([B] + R_3[E]) - k_4[A_2][B'] \tag{30}$$

$$\frac{d[A_1^*]}{dt} = k_2[A_2][B] + k_4[A_2][B'] + R_3k_2[A_2][E] - k_1^*[A_1^*][B] - R_3k_2^*[A_2^*][E] - k_3^*[A_1^*][B'] \tag{31}$$

$$\frac{d[A_2^*]}{dt} = k_1[A_1][B] + k_3[A_1][B'] + R_3k_1[A_1][E] - k_2^*[A_2^*][B] - R_3k_1^*[A_1^*][E] - k_4^*[A_2^*][B'] \tag{32}$$

$$\frac{d[B]}{dt} = -(k_1[A_1] + k_2[A_2])[B] - k_1^*[A_1^*][B] - k_2^*[A_2^*][B] \tag{33}$$

$$\frac{d[B']}{dt} = -(k_3[A_1] + k_4[A_2])[B'] - k_3^*[A_1^*][B] - k_4^*[A_2^*][B'] \tag{34}$$

$$\frac{d[E]}{dt} = (k_1[A_1] + k_2[A_2])[B] + k_1^*[A_1^*][B] + k_2^*[A_2^*][B] + (k_3[A_1] + k_4[A_2])[B'] + k_3^*[A_1^*][B'] + k_4^*[A_2^*][B'] - R_3[E]\{k_1[A_1] + k_2[A_2] + k_1^*[A_1^*] + k_2^*[A_2^*]\} \tag{35}$$

$$\frac{d[M]}{dt} = R_3[E]\{k_1[A_1] + k_2[A_2] + k_1^*[A_1^*] + k_2^*[A_2^*]\} \tag{36}$$

The concentration of the different species can be expressed in terms of conversion or fractional formation. Equations (37) to (43) define these variables. Aloph indicates allophanate (also represented by M in the equations above).

$$P_{A_i} = 1 - \frac{[A_i]}{2[A]_0}, .A_i = A, A_1, A_2, A_1^*, A_2^* \tag{37}$$

$$P_{B_T} = 1 - \frac{[B] + [B']}{2[B']_0 + 2[B_2]_0} \tag{38}$$

$$P_{B_2} = 1 - \frac{[B]}{2[B_2]_0} \tag{39}$$

$$P_{B'} = 1 - \frac{[B']}{2[B']_0} \tag{40}$$

$$P_E = 1 - \frac{[E]}{2[B]_0} \tag{41}$$

$$P_{Aloph} = 1 - \frac{[Aloph]}{2[B]_0} \tag{42}$$

$$P_{U_T} = P_E + P_{Aloph} \tag{43}$$

Macosko-Miller Probabilistic Recursive Model[34,35]

The methodology of the Macosko-Miller[34,35] approach to the modeling of molecular weight averages and branching is well established[34,35,38]. The method uses the statistical law of conditional expectation, Eq. (44), to calculate the expected mass of a population of polymer molecules. The core of the method is to calculate the expected mass values for each species. Using conditional probabilistic arguments and the concepts of ''looking in'' and ''looking out,'' Eqs. (48) to (54) are obtained.

$$E(Y) = E(Y|A)P(A) + E(Y|A^*)P(A^*) \tag{44}$$

The idea is to calculate M_w directly by using Eq. (45), where the expected values of molar mass of the molecules are calculated using Eq. (44) and physical arguments regarding the probabilities of reaction, $P(A)$, or no reaction, $P(A^*)$. M_n can be calculated from its definition, given by Eq. (47), where m_t is total mass and N is the number of moles of molecules. Subscripts ''0'' and ''b'' account for initial and present conditions, respectively.

M_x and w_X are molecular weight and mass fraction, respectively, of species X.

$$M_w = \sum_{i=1}^{N} w_{X_i} E(X_i) \tag{45}$$

where

$$w_{X_i} = \frac{M_{X_i} X_i}{\sum M_{X_i} X_i} \tag{46}$$

for $X_i = A_1, A_2, A_1^*, A_2^*, B, B', E, M$.

$$M_n = \frac{m_t}{N_0 - N_b} \tag{47}$$

Equations (48) to (68) for the expected masses of the different species ''looking in'' and ''looking out'' are interdependent. Although the main variables and symbols are explained within the text, the nomenclature section provides a detailed description of their meaning.

$$\begin{gathered} E(M_{X_i}) = E(M_{X_i}^{in}) + E(M_{X_i}^{out}) \\ X_i = A_1, A_2, A_1^*, A_2^*, B, B' \end{gathered} \tag{48}$$

$$E(M_E) = E(M_E^{in}) + (f_E - 1)E(M_E^{out}) \tag{49}$$

$$E(M_M) = E(M_M^{in}) + (f_M - 1)E(M_M^{out}) \tag{50}$$

$$\begin{gathered} E(M_{A_i}^{in}) = M_A + E(M_{A_i}^{out}) \\ A_i = A_1, A_2, A_1^*, A_2^* \end{gathered} \tag{51}$$

$$\begin{gathered} E(M_{X_j}^{in}) = M_{X_j} + E(M_{X_j}^{out}) \\ X_j = B, B', E, M \end{gathered} \tag{52}$$

$$E(M_{A_i}^{out}) = p_{A_i} \sum_j b_{X_j} E(M_{X_j}^{in}) \tag{53}$$

$$E(M_{X_i}^{out}) = p_{X_i} \sum_j a_{A_j} E(M_{A_j}^{in}) \tag{54}$$

where

$$a_{A_i} = \frac{[A_i]}{\sum_j [A_j]} \quad b_{X_j} = \frac{f_i X_i}{\sum_j f_j X_j}$$

The expected values of molar mass ''looking in'' are given by Eqs. (55) to (59) and the corresponding expected values of molar mass ''looking out'' by Eqs. (67) to (68).

$$E(M_{A_i}^{in}) = \frac{M_A(\phi_i \beta - 1) - p_{A_1}\gamma}{\alpha\beta - 1} \tag{55}$$

where

$$A_i = A_1, A_2, A_1^*, A_2^*$$

$$\phi_i = \phi_1 - \phi_4$$

$$E(M_B^{in}) = \frac{\alpha[M_B(\beta - p_B b_B) - p_B(\gamma - b_B M_B)] - (p_B M_A + M_B)}{\alpha\beta - 1} \tag{56}$$

$$E(M_{B'}^{in}) = \frac{\alpha[M_{B'}(\beta - p_{B'} b_{B'}) - p_{B'}(\gamma - b_{B'} M_{B'})] - (p_{B'} M_A + M_{B'})}{\alpha\beta - 1} \tag{57}$$

$$E(M_E^{in}) = \frac{1}{\alpha\beta - 1}\left\{\begin{array}{l}\alpha[M_E(\beta - (f_E - 1)p_E b_E)\\ -(f_E - 1)p_E(\gamma - b_E M_E)]\\ -((f_E - 1)p_E M_A + M_E)\end{array}\right\} \quad (58)$$

$$E(M_M^{in}) = \frac{1}{\alpha\beta - 1}\left\{\begin{array}{l}\alpha[M_M(\beta - (f_M - 1)p_M b_M)\\ -(f_M - 1)p_M(\gamma - b_M M_M)]\\ -((f_M - 1)p_M M_A + M_M)\end{array}\right\} \quad (59)$$

$$\alpha = p_{A_1}a_{A_1} + p_{A_1^*}a_{A_1^*} + p_{A_2}a_{A_2} + p_{A_2^*}a_{A_2^*} \quad (60)$$

$$\beta = p_B b_B + p_{B'} b_{B'} + (f_E - 1)p_E b_E + (f_M - 1)p_M b_M \quad (61)$$

$$\gamma = b_B M_B + b_{B'} M_{B'} + b_E M_E + b_M M_M \quad (62)$$

$$\phi_1 = p_{A_1^*}a_{A_1^*} + p_{A_2}a_{A_2} + p_{A_2^*}a_{A_2^*} + p_{A_1}(1 - a_{A_1}) \quad (63)$$

$$\phi_2 = (p_{A_1} - p_{A_2})a_{A_1} + (p_{A_1^*} - p_{A_2})a_{A_1^*} + (p_{A_2^*} - p_{A_2})a_{A_2^*} \quad (64)$$

$$\phi_3 = (p_{A_1} - p_{A_1^*})a_{A_1} + (p_{A_2} - p_{A_1^*})a_{A_2} + (p_{A_2^*} - p_{A_1^*})a_{A_2^*} \quad (65)$$

$$\phi_4 = (p_{A_1} - p_{A_2^*})a_{A_1} + (p_{A_2} - p_{A_2^*})a_{A_2} + (p_{A_1^*} - p_{A_2^*})a_{A_1^*} \quad (66)$$

$$E(M_{A_i}^{out}) = \frac{p_{A_i}(\beta M_A + \gamma)}{1 - \alpha\beta}, \quad A_i = A_1, A_2, A_1^*, A_2^* \quad (67)$$

$$E(M_{X_i}^{out}) = \frac{p_{X_i}(M_A + \alpha\gamma)}{1 - \alpha\beta}, \quad X_i = B, B', E, M \quad (68)$$

Calculation of Viscosity

Castro, Macosko, and Perry[39] examined the viscosity rise for three component polyurethane systems typical of REX and reaction injection molding (RIM), where phase separation plays a major role. Viscosity rise in polyurethane production has been found to be faster than that predicted by molecular weight considerations alone, and was largely attributed to the phase separation of hard segments during the polymerization. The effect of shear rate was studied by the group of Macosko. It was found that viscosity could be considered to be independent of shear rate. The viscosity relation can be greatly simplified, since temperature and extent of reaction effects can separated[36,39,40]. Thus, the general dependence of viscosity on temperature and conversion is given by Eq. (69).

$$\eta(T, X) = \eta_o(T)f(X) \quad (69)$$

η_0 is the initial viscosity ($\eta_0 = \eta(X = 0, \mathrm{T})$). This is modeled assuming linear weight additivity of the viscosities of the reactants, that is,

$$\eta_o = \Sigma\phi_i\,\eta_{oi} \quad (70)$$

where ϕ_i is the weight fraction of each component. The temperature dependence is assumed to be of the Arrhenius type, with $A_n = 4.1 \times 10^{-8}$ Pa-s and $E_n = 9.1402$ kcal/mol.

$$\eta_o = A_n \exp\left(\frac{E_n}{RT}\right) \quad (71)$$

It was found that Eq. (72) is adequate for polyurethane production systems[39].

$$\eta = \eta_o\left(\frac{Cg}{Cg - X}\right)^{\alpha+\beta X}, \quad \alpha = 4,\ \beta = -2 \text{ and } Cg = 0.85. \quad (72)$$

Additional viscosity rise experiments should be carried out to determine the dependence of A_n, E_n, C_g, α, and β with temperature and conversion, in order to apply Eq. (72).

RESULTS AND DISCUSSION

The polymerization system studied in this paper was the REX copolymerization of (MDI)/polyester/1,4-butanediol. The kinetic and model parameters were taken from the

TABLE 1
Initial conditions for copolymerization of MDI, polyester, and 1,4-butanediol[36]

Variable	Value	Units
Temperature	30, 50, or 90	°C
$[A_1A_2]_0$	1.5261	mol L^{-1}
$[B_2]_0$	0.3052	mol L^{-1}
$[B'_2]_0$	1.221	mol L^{-1}

TABLE 2
Molecular weight parameters[36]

Parameter	Value	Units
M_A	250	g mol^{-1}
M_B	2500	g mol^{-1}
$M_{B'}$	90	g mol^{-1}
M_E	59	g mol^{-1}
M_M	101	g mol^{-1}
f_E	3	
f_M	4	

literature[36]. The polymerization conditions, molecular weights of the different reactive species, and other parameters are summarized in Tables 1 to 3. Figure 2 shows the sequence of calculations (flow diagram) followed to model the extruder performance.

In order to test the implementation of the polymerization kinetic model, the extruder was simulated under isothermal conditions, thus resembling the behavior of a batch reactor, which made possible to compare model simulations for isothermal REX operation with bulk polymerization in a batch reactor. Figure 3 shows reported experimental data[41] of weight average molecular weight vs. conversion at three different temperatures, from 30° to 90°C. The weight-average molecular weight data reported by Castro[41] were obtained using an equation developed by López-Serrano et al.[42]. That equation is indeed based on the Macosko-Miller linear approach[34,35], considering three monomers as in this paper, but neglecting branching and crosslinking reactions. Experimental data on the extent of reaction were inserted into that equation to obtain the corresponding M_w values. Castro[41] reported that gelation occurred at approximately 85% hydroxyl conversion, but he based his statement on the observation of a plot of viscosity vs. conversion that seemed to diverge at around that conversion level. Figure 4 shows predicted profiles of weight-average molecular weight vs. total hydroxyl conversion at the same three temperatures as Castro[41], calculated with the model by Vivaldo-Lima et al.[36], coupled to the extruder equations described before. In all the three cases, the profiles overlap. The final conversion reached depends on temperature. The higher the temperature chosen, the higher conversion levels are reached. The gelation point takes place at a calculated 78% hydroxyl conversion. The difference between experimental and calculated values is relatively small, but it has to be considered that some kinetic rate constants were estimated using Castro's experimental data. Both models have the same behavior in the pre-gelation period, as shown in Figure 5. Macosko[43] has studied these systems, and he reported that the gelation point is independent of temperature, although this can be true only over a limited temperature range (30–90°C).

Model predictions of number and weight average molecular weights along the extruder at several temperatures are shown in Figs. 6 and 7, respectively. It is observed that molecular weight increases with temperature, and that the gelation point takes place sooner when temperature is higher. The gelation point takes place at chambers 90, 107, and 146 at temperatures of 90°, 85°, and 80°C, respectively, at the same value of 78% total hydroxyl conversion, for the three cases. Calculations of the polydispersity index (PDI) at different temperatures, in the range of 30° to 90°C, are shown in Fig. 8. It is observed that at low conversions (in the region of 1 to around 20 CSTRs) PDI decreases with conversion, and the values of PDI are slightly lower when temperature is higher. At 30° and 50°C the decreasing tendency with conversion continues up to high conversions. However, at 75° and 90°C, the trend changes, with PDI increasing with conversion, and reaching higher values when

TABLE 3
Kinetic rate constants[36]

Parameter	30°C	50°C	90°C	Units or comments
k_1	0.02924	0.0795	0.45	L mol^{-1} min^{-1}
k_2	0.02924	0.0795	0.45	L mol^{-1} min^{-1}, assumed equal to k_1
k_3	0.0106 ± 0.0002	0.0168 ± 0.0003	0.3163 ± 0.02	L mol^{-1} min^{-1}, ("error in variables method," EVM)
k_4	0.0106 ± 0.0002	0.0168 ± 0.0003	0.3163 ± 0.02	L mol^{-1} min^{-1}, assumed equal to k_3
k_1^*	0.0001	0.0068 ± 0.0003	1.25×10^{-2}	L mol^{-1} min^{-1}, EVM (zero included in confidence interval at 30° and 90°C)
k_2^*	0.0001	0.0068 ± 0.0003	1.25×10^{-2}	L mol^{-1} min^{-1}, assumed equal to k_1^*
k_3^*	0.0072	0.0263 ± 0.0008	0.019	L mol^{-1} min^{-1}, EVM (zero included in confidence interval at 30° and 90°C)
k_4^*	0.0072	0.0263 ± 0.0008	0.019	L mol^{-1} min^{-1}, assumed equal to k_3^*
R_3	0.00263	0.00263	0.00263	Gupta and Kumar[37]

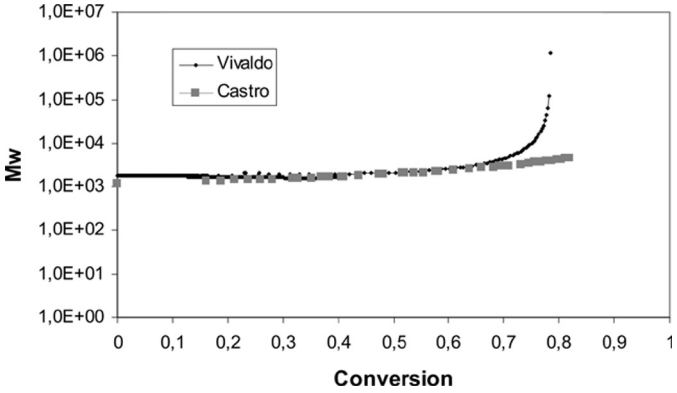

FIG. 5. Copolymerization of MDI/polyol/1,4-Butanediol. Comparison of model predictions, with initial conditions listed in Table 1.

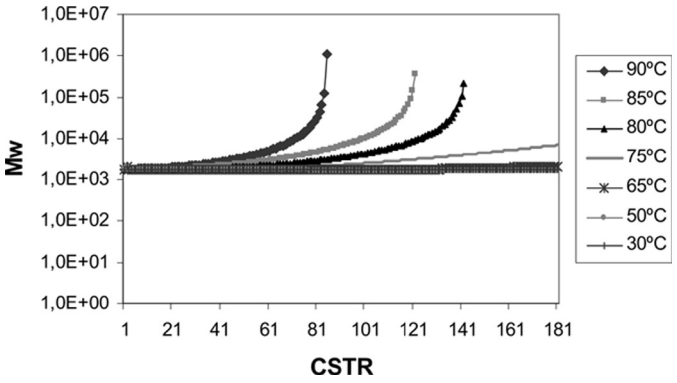

FIG. 6. Model predictions of weight-average molecular weight at different temperatures, as a function of position along the extruder, at 25 rpm and 40 g min^{-1}, and initial conditions from Table 1.

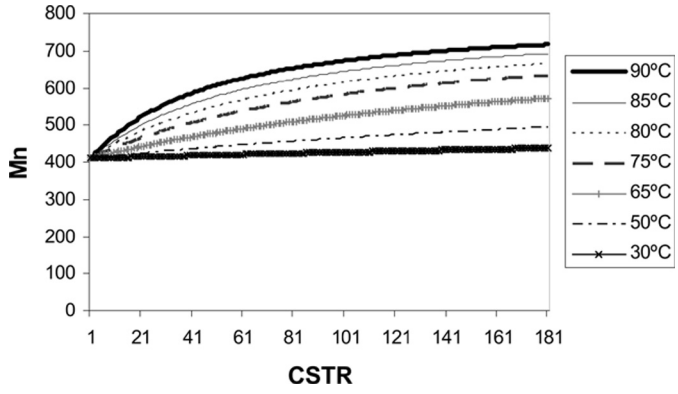

FIG. 7. Model predictions of number average molecular weight at different temperatures, as a function of position along the extruder, at 25 rpm and 40 g min^{-1}, and initial conditions from Table 1.

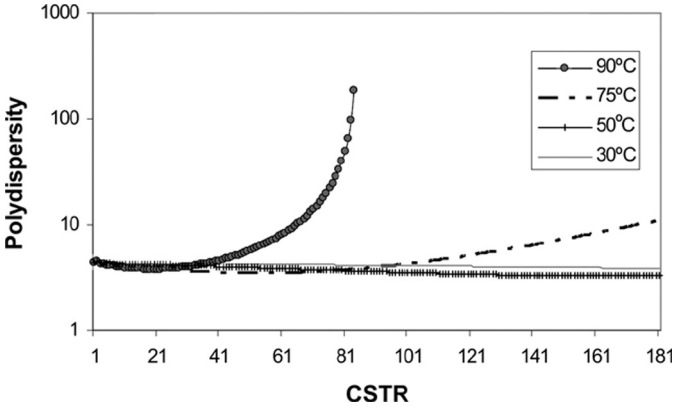

FIG. 8. Model predictions of the polydispersity index as a function of position along the extruder, at 25 rpm and 40 g min^{-1}, and initial conditions from Table 1.

temperature is higher. At 75°C PDI increases with conversion, without reaching the gelation point, but at 90°C the gelation point is reached around CSTR number 90.

Viscosity is the most important material property in polymer-processing operations involving flow. Viscosity variation along the extruder at three different temperatures is shown in Fig. 9. As in the case of weight average molecular weight, at slow conversions viscosity is reduced when temperature is increased, but at a given temperature, as conversion increases, viscosity also increases. Once again, it is observed that the gelation point is reached around CSTR number 90, at 90°C, and that there is no gel formation at 30° and 50°C. It is also observed in Fig. 9 that a significant change on behavior occurs between 50° and 90°C.

Figures 10 and 11 show generated pressure profiles along the extruder, at different temperatures and screw rotational rates, respectively. It is observed in Fig. 10 that increasing temperature causes to have an increasing pressure profile after CSTR number 40, reaching the gelation point at approximately CSTRs 150 and 90, at 80° and

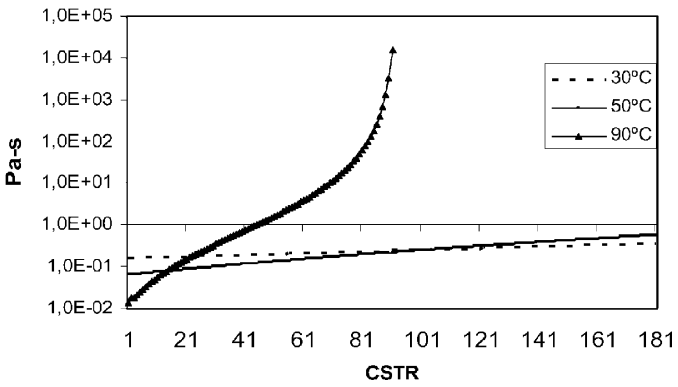

FIG. 9. Viscosity variation along the extruder at 25 rpm, 40 g min^{-1}, different temperatures, and initial conditions from Table 1.

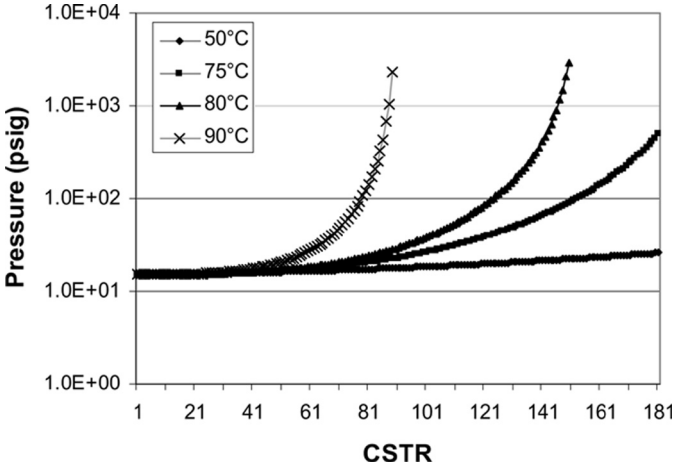

FIG. 10. Predicted pressure along the extruder at 25 rpm, 40 g min^{-1}, different temperatures, and initial conditions from Table 1.

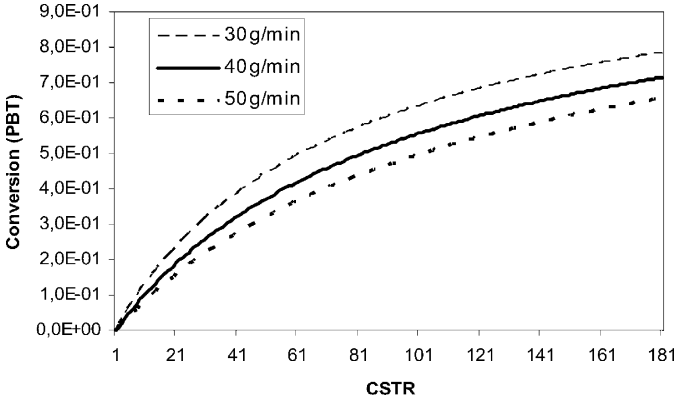

FIG. 12. Effect of the throughput on overall diol conversion, for the initial conditions of Table 1, 25 rpm, and 75°C.

90°C, respectively. At 50° and 75°C the pressure profile increases with conversion (extruder length or CSTR number), but the gelation point is not reached within the length of the extruder (not reached by CSTR number 181). If the gelation point was to be avoided, then the extruder should not be operated in an isothermal way above 75°C. Figure 11 shows that increasing the screw rotational speed produces higher pressure development along the extruder, when temperature is constant at 75°C. It is also observed in Fig. 11 that increasing the screw rotational speed seems to anticipate the gelation point, a situation that will be corroborated later in this paper, when the effect of speed of rotation on weight average molecular weight is analyzed. This effect can be understood by considering that the material balances depend on the different flows entering and leaving a CSTR unit, including the leakage terms. Since the leakage flows depend on the pressure gradient, it then turns out that the pressure gradient will affect conversion of monomers into polymer, reaching higher conversions when the pressure gradient is higher and, therefore, reaching sooner the gelation point.

Figure 12 shows the effect of the throughput on the overall diol conversion. It is observed that increasing the throughput causes a reduction on the overall diol conversion. This is caused by the increase on the residence time with decreasing the throughput, which allows to reach higher conversions, since the molecules spend more time in a given element (CSTR). The higher conversion achieved when the throughput is reduced causes the increase on weight average molecular weight, to the point of reaching the gelation point at element 180, when the throughput is of 30 g min^{-1}, T = 70°C and the speed of rotation is 25 rpm, as shown in Fig. 13.

Figure 14 shows the effect of the speed of rotation on the weight average molecular weight. It is observed that increasing the speed of rotation decreases the weight average molecular weight, which can be explained considering that when the speed of rotation is faster, the polymer molecules will spend less time at a given element (equivalent to reducing

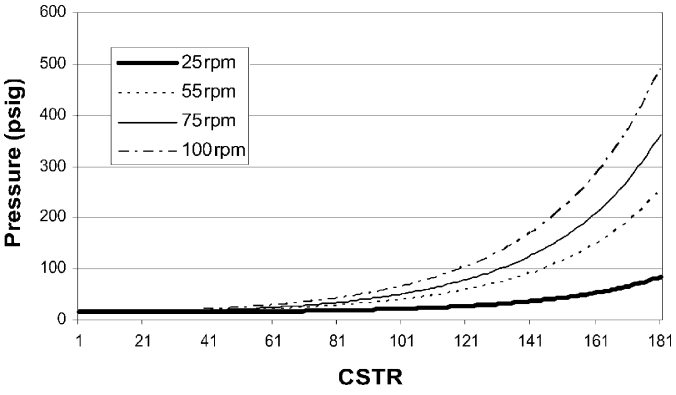

FIG. 11. Effect of screw rotational rate on the generated pressure, for the initial conditions of Table 1, 75°C, and 40 g min^{-1}.

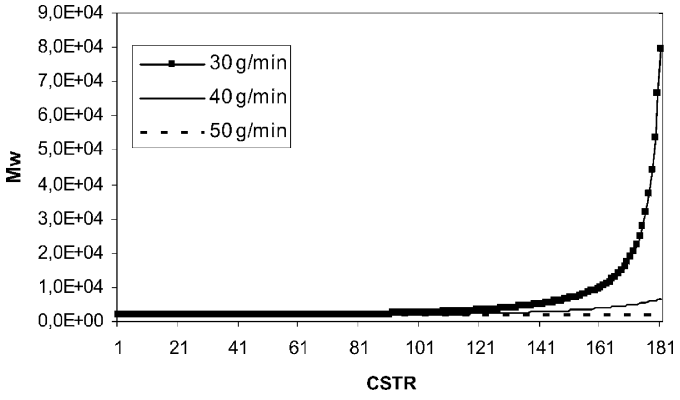

FIG. 13. Effect of the throughput on the weight average molecular weight, for the initial conditions of Table 1, 25 rpm, and 70°C.

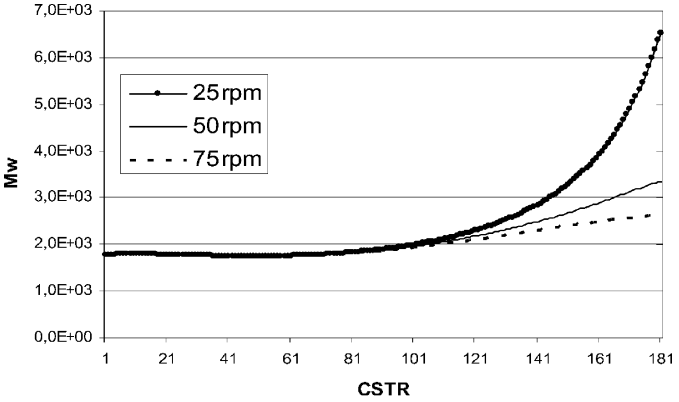

FIG. 14. Effect of screw rotational rate on weight average molecular weight, for the initial conditions of Table 1, 70°C, and 4 g min^{-1}.

the residence time in the CSTRs), thus reaching lower conversion, and lower weight average molecular weight.

Finally, Fig. 15 shows the effect of the stoichiometric imbalance ratio (SIR) on the weight average molecular weight, when the extruder is operated isothermally at 70°C, 25 rpm, and 40 g min^{-1}. It is observed that when the amount of −NCO (isocyanate) functional groups is increased, with respect to the amount of −OH (hydroxyl) functional groups, the weight average molecular weight is increased, reaching the gelation point sooner. This can be understood by considering that allophanate formation (the reaction that will allow branching and crosslinking) is produced by the reaction of the −NCO functional group with the proton from the urethane functional group that results from the reaction between isocyanate and hydroxyl functional groups; namely, that an excess of isocyanate functional groups promotes the formation of more allophanate units, and the production of allophanate units promotes branching and crosslinking, reactions that increase the weight average molecular weight, and make possible to get a gel molecule.

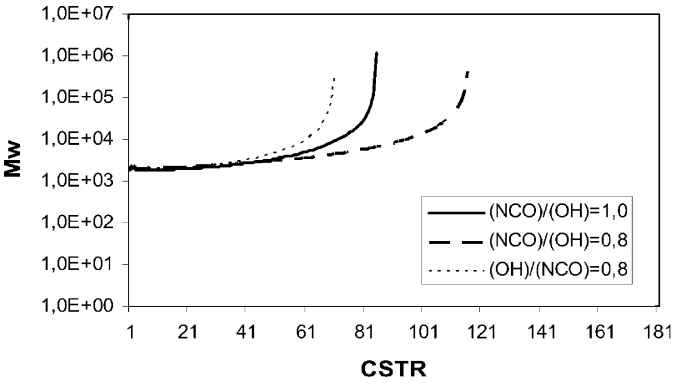

FIG. 15. Effect of the stoichiometric imbalance ratio on the weight average molecular weight along the extruder, at 25 rpm and 40 g min^{-1}.

CONCLUDING REMARKS

A simple mathematical model for nonlinear polyurethane production by reactive extrusion was presented. This was made possible by coupling an ideal "series of CSTRs" reactor model with a kinetic-probabilistic model for polyurethane production, which includes branching and crosslinking reactions, and the possibility of reaching the gelation point. The simple mathematical structure, yet good enough representation of the actual extruder performance, makes it attractive for industrial use.

The effect of the most important parameters in reactive extrusion, such as temperature, screw rotational rate, throughput, and stoichiometric imbalance ratio, on the main responses (monomer conversion, weight average molecular weight, viscosity, and pressure), along the extruder length, is well captured by the model.

Although specialized CFD software for polymer processing is available in the market, such as Fluent or Femlab, when the reaction terms of the constitutive equations consist of a complex reaction mechanism, it is still useful to use simple flow models, coupled to polymerization kinetic models from intermediate to high degrees of complexity.

NOMENCLATURE

For the Kinetic Model

[ ], [ ]$_0$	concentration, where subscript 0 indicates value at initial conditions, mol L^{-1}
A	isocyanate functional group
A_2	diisocyanate molecule
a_{Ai}	molar fraction of isocyanate functional group, as defined in Eq. (54)
Aloph	allophanate functional group (also represented by M)
B	hydroxyl functional group
B_2	diol molecule of high molecular weight (polyol)
B'_2	diol molecule of low molecular weight (1,4-butanediol)
BDO	1,4-butanediol
b_{Xi}	quantity defined by Eq. (53)
E	urethane functional group
$E(X_i)$	expected mass of species X_i, kg $kmol^{-1}$
f_{Xi}	functionality of species X_i, X_i = E, M
k_i, k_i^*	kinetic rate constants, where superscript * indicates reactivity of a functional group bound to a polymer molecule and subscript or superscript 0 denotes value at initial conditions. L mol^{-1} min^{-1}
m_t	total mass, kg
M	allophanate functional group (also represented as Aloph)
M_n	number average molecular weight, kg $kmol^{-1}$
M_X	molar mass of species X, kg $kmol^{-1}$
M_w	weight-average molecular weight, kg $kmol^{-1}$

N_0, N_b number of molecules at initial and present conditions, respectively
p_X extent of reaction (probability of reaction) of species X, as defined in Eqs. (37) to (43)
R_3 proportionality constant between rates of allophanate and urethane formation
t time, min
T temperature, °C
$[U_T]$ total polymer concentration, mol L^{-1}
w_X mass fraction of species X, as defined in Eq. (46)

Greek Letters

α intermediate variable in the Macosko-Miller model defined by Eq. (60)
β intermediate variable in the Macosko-Miller model defined by Eq. (61)
Φ_i intermediate variable in the Macosko-Miller model, i = 1,2,3,4 as defined in Eqs. (63) to (66)
γ intermediate variable in the Macoko-Miller model defined by Eq. (62)

For the Extrusion Model

[ ] concentration, mol L^{-1}
B pitch of the screw
Be axial width of the flight at the outer radius
Cp heat capacity, J g^{-1} K^{-1}
D screw diameter, m
H height of the chamber, m
ΔH_r reaction enthalpy, J mol^{-1}
h heat transfer coefficient, W m^{-2} K^{-1}
Kr reaction constant, L mol^{-1} min^{-1}
N rotational rate, min^{-1}
ΔP pressure difference between two consecutive chambers, Psig
Q throughput, m^3 min^{-1}
Q_c calender leak, m^3 min^{-1}
Q_f flight leak, m^3 min^{-1}
Q_{tot} total leak flow, m^3 min^{-1}
Q^i leak flow in the i-th chamber, m^3 min^{-1}
Q_l side leak, m^3 min^{-1}
Q_t tetrahedron leak, $m^3 min^{-1}$
Q_{th} theoretical throughput, m^3 min^{-1}
R_e radius of the screw, m
T temperature, °C
T_w wall temperature, °C
t time, min
V_c chamber volume, m^3

Greek Letters

α overlap angle
β angular coordinate
δ flight gap width
ε side gap width
η viscosity, Pa s
σ chamber gab width, m
ψ screw flank angle

ACKNOWLEDGMENTS

The authors wish to acknowledge financial support through research project grants from the National Council for Science and Technology (CONACYT) of Mexico to E.V.-L. and O.M., and the graduate scholarship granted to R.O.V. by CONACYT. Financial support from DGAPA-UNAM, through project PAPIIT IN106302, is also acknowledged.

REFERENCES

1. Rauwendal, C. *Polymer Extrusion*, 3rd Ed., Haser: Vienna, New York, 1994.
2. White, J.L. *Twin Screw Extrusion Technology and Principles*, Hanser: New York, 1991.
3. Vergnes, B.; Souveton, G.; Delacour, M.L.; Ainser, A. Experimental and theoretical study of polymer melting in corotating twin screw extruders. Inter. Polym. Proc. **2001**, *16* (4), 351–362.
4. Van der Goot, A.J.; Hettema, R.; Janssen, L.P.B.M. The working domain in reactive extrusion. 1. The effect of the polymer melt viscosity. Polym. Eng. Sci. **1997**, *37* (7), 511–518.
5. Potente, H.; Kretschmer, K. Simulating and evaluation of compounding processes. Macromolecular Material and Engineering **2002**, *287* (11), 758–772.
6. Potente, H. Simulation of processing behaviour of screw machines. Kunststoffe-plast Europe **1999**, *89* (1), 83.
7. Janssen, L.P.B.M.; Rozendal, P.F.; Hoogstraten, H.W.; Cioffi, M. A dynamic model accounting for oscillating behavior in reactive extrusion. Inter. Polym. Proc. **2003**, *18* (3), 277–284.
8. Janssen, L.P.B.M.; Rozendal, P.F.; Hoogstraten, H.W.; Cioffi, M. A dynamic model for multiple steady states in reactive extrusion. Inter. Polym. Proc. **2001**, *16* (3), 263–271.
9. de Graaf, R.A.; Rohde, M.; Janssen, L.P.B.M. A novel model predicting the residence time distribution during reactive extrusion. Chem. Eng. Sci. **1997**, *52* (23), 4345–4356.
10. Thompson, N.; Puaux, J.P.; Hrymak, A.N.; Hamielec, A.E. Modeling the residence time distribution of a nonintermeshing twin-screw extruder. Inter. Polym. Proc. **1995**, *10* (2), 111–119.
11. Potente, H.; Tobben, W.H.; Heinrich, D.; Pape, J. Screw concepts: Influence of the plasticizing unit on the processing of PET. Kunststoffe-plast Europe **2003**, *93* (1), 56.
12. Potente, H.; Pape, J. Flexible use of single-screw extruders through multiple-process optimization. Macromolecular Material and Engineering **2002**, *287* (11), 784–790.
13. Potente, H.; Ridder, H. Pressure/throughput behaviour of a single-screw plasticizing unit in consideration of wall slippage. Inter. Polym. Proc. **2002**, *17* (2), 102–107.
14. Flecke, J.; Potente, H.; Kretschmer, K. A physico-mathematical model for the dispersion process in a co-rotating intermeshing twin screw extruder. J. Reinforced Plastics and Composites **2002**, *21* (6), 507–515.
15. Vergnes, B.; Della Valle, G.; Delamare, L. A global computer software for polymer flows in corotating twin screw extruders. Polym. Eng, Sci. **1998**, *38* (11), 1781–1792.
16. Berzin, F.; Vergnes, B.; Dufosse, P.; Delamare, L. Modeling of peroxide initiated controlled degradation of polypropylene in a twin screw extruder. Polym. Eng. Sci. **2000**, *40* (2), 344–356.
17. Carneiro, O.S.; Covas, J.A.; Vergnes, B. Experimental and theoretical study of twin-screw extrusion of polypropylene. J. Appl. Polym. Sci. **2000**, *78* (7), 1419–1430.

18. Poulesquen, A.; Vergnes, B.; Cassagnau, P.; Gimenez, J.; Michel, A. Polymerization of epsilon-caprolactone in a corotating twin screw extruder-experimental study and modelling. Inter. Polym. Proc. **2001**, *16* (1), 31–38.
19. Janssen, L.P.B.M. *Twin Screw Extrusion*, Elsevier Science Publishers: New York, 1978.
20. Janssen, L.P.B.M. On the stability of reactive extrusion. Polym. Eng. Sci. **1998**, *38* (12), 2010–2019.
21. Van der Goot, A.J.; Poorter, O.; Janssen, L.P.B.M. Determination of the degree of fill in a counter-rotating twin screw extruder. Polym. Eng. Sci. **1998**, *38* (7), 1193–1198.
22. Van der Goot, A.J.; Klaassens, S.A.; Janssen, L.P.B.M. The working domain in reactive extrusion. 1. The effect of the polymerization rate. Polym. Eng. Sci. **1997**, *37* (3), 519–528.
23. Bouilloux, A.; Macosko, C.W. Urethane polymerization in a counter-rotating twin-screw extruder. Ind. Eng. Chem. Res. **1991**, *30* (11), 2431–2436.
24. Ganzeveld, K.J.; Janssen, L.P.B.M. A mixing model for multicomponent reactions in twin screw extruders applied to the polymerization of urethanes. Polym. Eng. Sci. **1992**, *32* (7), 457–466.
25. Xanthos, M. *Reactive Extrusion, Principles and Practice*, Hanser Gardner Publications Inc.: Cincinnati, 1992.
26. Hyun, M.E.; Kim, S.C. A study on the reactive extrusion process of polyurethane. Polym. Eng. Sci. **1988**, *28* (11), 743–757.
27. Stuber, N.P. Studies of continuous methyl methacrylate polymerization in a twin-screw extruder. Ph.D. Thesis, University of Minnesota, 1986.
28. Jongbloed, H.A.; Mulder, R.K.S.; Janssen, J.P.B.M. The copolymerization of methacrylates in a counter-rotating twin-screw extruder. Polym. Eng. Sci. **1995**, *35* (7), 587–597.
29. Ganzeveld, K.J.; Janssen L.P.B.M. Scale-up of counter-rotating closely intermeshing twin screw extruder without and with reactions. Polym. Eng. Sci. **1990**, *30* (23), 1529–1536.
30. Cassagnau, P.; Nietsch, T.; Michel, A. Bulk and dispersed phase polymerization of urethane in twin screw extruders. Inter. Polym. Proc. **1999**, *14* (2), 144–151.
31. Cassagnau, P.; Nietsch, T.; Bert, M.; Michel, A. Reactive blending by in situ polymerization of the dispersed phase. Polymer **1999**, *40* (1), 131–138.
32. DeLoor, A.; Cassagnau, P.; Michel, A.; Verges, B. Mechanical properties of a polymer blend obtained through in situ crosslinking of the dispersed phase. J. Appl. Polym. Sci. **1997**, *63* (10), 1385–1390.
33. DeLoor, A.; Cassagnau, P.; Michel, A.; Delamare, L.; Verges, B. Reactive blending in a twin screw extruder—experimental and theoretical approaches. Inter. Polym. Proc. **1996** *11* (2), 139–146.
34. Macosko, C.W.; Miller D.R. A new derivation of average molecular weight of nonlinear polymers. Macromolecules **1976**, *2* (9), 199–206.
35. Macosko, C.W.; Miller D.R. A new derivation of post gel properties of network polymers. Macromolecules **1976**, *2* (9), 206–211.
36. Vivaldo-Lima E.; Luna-Bárcenas, G.; Flores-Tlacuahuac, A.; Cruz M. A.; Manero O. Modelling of non-linear polyurethane production in batch reactors using a kinetic-probabilistic approach. Ind. Eng. Chem. Res. **2002**, *41*, 5207–5219.
37. Gupta, S.K.; Kumar, A. *Reaction Engineering of Step Growth Polymerization*, Plenum Press: New York, 1987.
38. Dotson, N.A.; Galván, R.; Laurence, R.L.; Tirrel, M. *Polymerization Process Modeling*, Wiley-VCH: New York, 1996.
39. Castro, J.M..; Macosko, C.W.; Perry, S.J. Viscosity changes during urethane polymerization with phase separation. Polym. Commun. **1984**, *25*, 82–87.
40. Castro, J.M.; López Serrano, F.; Camargo, R.E.; Macosko, C.W.; Tirrel, M. Onset of phase separation in segmented urethane polymerization. J. Appl. Polym. Sci. **1981**, *26*, 2067–2076.
41. Castro, J.M. Ph.D. Mold filling and curing studies for the polyurethane RIM process. Thesis, Department of Chemical Engineering, University of Minnesota, Minneapolis, MN, 1980.
42. López-Serrano, F.; Castro, J.M.; Macosko, C.W.; Tirrel, M. Recursive approach to copolymerization statistics. Polymer **1980**, *21*, 263–273.
43. Macosko, C.W. *Fundamentals of Reaction Injection Molding*. Hanser: Munich, 1989.